PNAS RESEARCH ARTICLE | EVOLUTION BIOPHYSICS AND COMPUTATIONAL BIOLOGY

Suppressors of fixation can increase average fitness beyond amplifiers of selection

Nikhil Sharma[a,1] and Arne Traulsen[a,1]

Edited by Kenneth Wachter, University of California, Berkeley, CA; received March 28, 2022; accepted August 3, 2022

Evolutionary dynamics on graphs has remarkable features: For example, it has been shown that amplifiers of selection exist that—compared to an unstructured population—increase the fixation probability of advantageous mutations, while they decrease the fixation probability of disadvantageous mutations. So far, the theoretical literature has focused on the case of a single mutant entering a graph-structured population, asking how the graph affects the probability that a mutant takes over a population and the time until this typically happens. For continuously evolving systems, the more relevant case is that mutants constantly arise in an evolving population. Typically, such mutations occur with a small probability during reproduction events. We thus focus on the low mutation rate limit. The probability distribution for the fitness in this process converges to a steady state at long times. Intuitively, amplifiers of selection are expected to increase the population's mean fitness in the steady state. Similarly, suppressors of selection are expected to decrease the population's mean fitness in the steady state. However, we show that another set of graphs, called suppressors of fixation, can attain the highest population mean fitness. The key reason behind this is their ability to efficiently reject deleterious mutants. This illustrates the importance of the deleterious mutant regime for the long-term evolutionary dynamics, something that seems to have been overlooked in the literature so far.

evolutionary graph theory | mutation-selection balance | low mutation rates | deleterious mutant regime

Significance

Spatial structure can substantially affect evolutionary dynamics. These dynamics are usually studied through the fixation process of a single mutation. This allows one to classify structures, e.g., as amplifiers, which enhance the effect of selection. Here, we provide a model integrating the fixation process of single mutations into the long-term evolutionary dynamics, characterized by a balance between mutation and selection. Certain structures that do not perform well for single fixation events can perform very well at longer time scales due to their ability to reject deleterious mutants. This means that a structure can be improved by only increasing its ability to reject deleterious mutants—the increase of its ability to fix advantageous mutations is less central than previously thought.

Understanding how spatial structures can affect evolutionary dynamics has been of interest to evolutionary biologists for a long time. More than a decade ago, a framework known as evolutionary graph theory was introduced (1). The primary quantity of interest has been the fixation probability of a mutant on graphs, which is the probability that a mutant with given fitness takes over the rest of the wild-type population (2–6).

Fixation probability is a central concept in evolutionary biology, as it determines the rate of evolution in the low mutation rate regime (7, 8). Spatial structure tweaks the strength of selection and genetic drift (9, 10). As a consequence, some graphs have higher probability of fixation than others for a mutant with a given fitness value. Of particular interest are those graphs that increase the fixation probabilities for advantageous mutants and decrease the fixation probabilities for disadvantageous mutants—so-called amplifiers of selection. While initially, amplifiers seemed to be special structures (1), it turned out that under Birth–death (Bd) updating, most random networks are amplifiers of selection (11).

However, fixation describes evolutionary dynamics only on a relatively short time scale. In the long run, additional mutants will arise, and the population will eventually reach a steady state in terms of fitness (12). A model that investigates such long evolutionary trajectories in graph-structured populations has been missing so far. This problem has been studied via a process where two types of individuals with fixed fitness values compete with each other, leading to a mutation–selection balance in the steady state (13), but not for the case of continuously arising mutations with a potentially infinite number of types. The neutrality counterpart of this problem has been investigated in ref. 14, where equilibrium properties are shown to be independent of the population structure.

In evolutionary graph theory, every node of a graph is an individual. If an individual produces an offspring, the offspring is placed in a neighboring node. We focus on undirected and unweighted graphs, where all neighboring nodes are chosen with the same probability. Graphs can be classified based on their fixation probability, as compared to that of the complete graph. The fixation probability of a mutant with fitness f' appearing in a population with fitness f on a complete network C (corresponding to a well-mixed population) is given by

$$\phi_C^{\mathcal{I}}(f',f) = \phi_C(f',f) = \frac{1-\frac{f}{f'}}{1-\left(\frac{f}{f'}\right)^N}. \quad [1]$$

Author affiliations: [a]Department of Evolutionary Theory, Max Planck Institute for Evolutionary Biology, 24306 Plön, Germany

Author contributions: N.S. and A.T. designed research; N.S. and A.T. performed research; N.S. contributed new reagents/analytic tools; N.S. and A.T. analyzed data; and N.S. and A.T. wrote the paper.

The authors declare no competing interest.

This article is a PNAS Direct Submission.

[1]To whom correspondence may be addressed. Email: nsharma@evolbio.mpg.de or traulsen@evolbio.mpg.de.

Published September 6, 2022.

In this case, all nodes are equivalent, and it does not matter where the mutation occurs. In the general case, the fixation probability depends crucially upon the node where the mutant first arises (15). In Eq. **1**, $\mathcal{I}$ denotes this initialization scheme, according to which a mutant arises on the network. To be specific, $\mathcal{I}$ is the probability distribution represented by a row vector of size N where element i is the probability with which a mutant arises at node i in a homogenous background. In the simplest case, this is a uniform probability—this case is typically referred to as uniform initialization.

Based on fixation probabilities and the initialization scheme, graphs typically fall into three categories (11):

- An amplifier of selection is a graph G that increases the fixation probability of an advantageous mutant and decreases the fixation probability of a disadvantageous mutant compared to a complete graph, $\phi_G^{\mathcal{I}}(f',f) > \phi_C^{\mathcal{I}}(f',f)$ for $f' > f$ and $\phi_G^{\mathcal{I}}(f',f) < \phi_C^{\mathcal{I}}(f',f)$ for $f' < f$.
- A suppressor of selection is a graph G that decreases the fixation probability of an advantageous mutant and increases the fixation probability of a disadvantageous mutant compared to a complete graph, $\phi_G^{\mathcal{I}}(f',f) < \phi_C^{\mathcal{I}}(f',f)$ for $f' > f$ and $\phi_G^{\mathcal{I}}(f',f) > \phi_C^{\mathcal{I}}(f',f)$ for $f' < f$.
- An isothermal graph is a graph G that has the same fixation probability as the complete graph, $\phi_G^{\mathcal{I}}(f',f) = \phi_C^{\mathcal{I}}(f',f)$ for all f' and f. In particular, any graph where the number of links for each node is the same is an isothermal graph for uniform initialization [in the more general case of weighted graphs, where mutants are placed on neighboring nodes with different probabilities (16). For a structure to be an isothermal graph, every node should have equal temperature. The temperature of a node i is equal to the sum of the incoming link weights w_{ji}, $\sum_{j=1}^{N} w_{ji}$].

For later purposes, we introduce a fourth type (11, 17), suppressors of fixation:

- A suppressor of fixation is a graph G that reduces the fixation probability for both advantageous and disadvantageous mutants, $\phi_G^{\mathcal{I}}(f',f) < \phi_C^{\mathcal{I}}(f',f)$ for all $f' \neq f$. These graphs are also called reducers of fixation (18).

The definition for isothermal networks has originally been defined for a uniform initialization scheme. In general, such a definition would depend on the details of the update rule (19). The classifications for amplifiers and suppressors above have also been developed for uniform mutant initialization. For other initialization schemes—for example, temperature initialization—the classifications become less straightforward, especially near neutrality (20).

Model

In order to generate any evolutionary dynamics, we must choose an update mechanism. We focus on the Bd update rule, where, first, an individual is selected at random, but proportional to fitness. This individual produces an offspring, which is placed in one of the neighboring nodes. We assume that the offspring is mutated with a small probability μ and identical to its parent with probability $1-\mu$. The state of a population is represented by a fitness vector $\mathbf{f} = (f_1, f_2, \cdots, f_{N-1}, f_N)^{\mathrm{T}}$, where f_i is the fitness of an individual at node i. When an offspring is mutated, we choose its fitness f' from a continuous bounded distribution $\rho(f',f)$, where f is the parent's fitness and $f_{\min} \leq f' \leq f_{\max}$ (Fig. 1*A*).

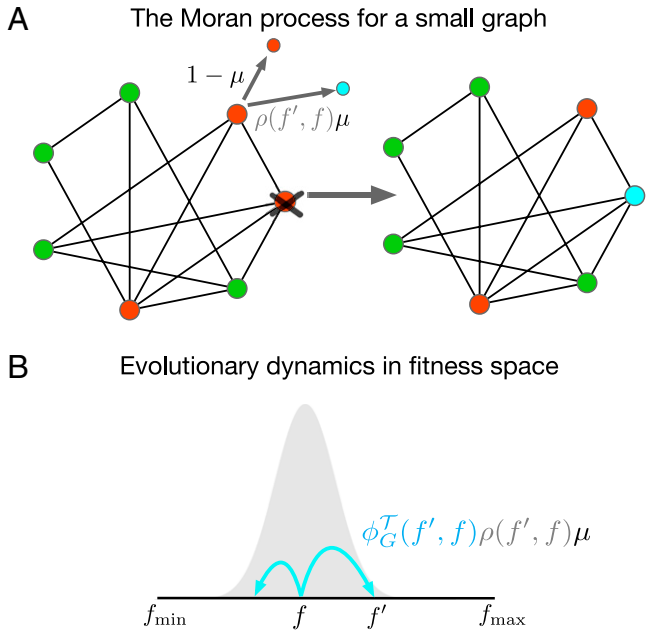

Fig. 1. Moran Birth-death (Bd) with continuous mutation on a graph. (*A*) The Moran Bd update mechanism with continuous mutation is shown for a small graph. An individual is selected to reproduce with probability proportional to its fitness. The offspring mutates with probability μ, and its fitness f' is sampled from a distribution $\rho(f',f)$, where f is the parent's fitness. A neighboring individual is then chosen for death at random among the neighboring nodes, and the offspring is placed in the empty node. We work in the low mutation rate approximation where μ is very small, such that only a single type is typically present in the population. (*B*) Evolutionary dynamics in fitness space. For low mutation rates, the evolutionary dynamics effectively becomes a biased random walk on the fitness space. The transition rates depend on the mutation rate μ, the fitness distribution of the mutant offspring $\rho(f',f)$ (shown in gray), and the fixation probabilities $\phi_G^{\mathcal{T}}(f',f)$.

Instead of looking into the full evolutionary trajectory of the system, we focus only on the fitness distribution in the steady state. As this is difficult for arbitrary mutation rates, we concentrate on the low mutation rate regime here. In this regime, the entire population effectively moves as a point (most of the time) in the fitness space. Typically, every individual in a population has the same fitness. Thus, the state of the population can be labeled by a single fitness value, f. This is a good approximation if the time between two successive mutations is sufficiently high that a new mutant either gets extinct or takes over the entire population before the next mutation arises. Thus, our model describes sequential fixation (21) (Fig. 1*B*). We are mainly interested in the dynamics of probability density $P_G(f,t)$. One important observation is that mutations do not arise in all nodes with uniform probability, but mostly in those nodes that have more incoming links. This is captured by the idea of "temperature initialization" (20), where the probability that a mutation arises is proportional to the temperature of a node i, $\sum_{j=1}^{N} w_{ji}$. In the case of unweighted networks, $w_{ji} = 1$ if a link between j and i exists; otherwise, $w_{ji} = 0$. With this, we can write down the master equation of the corresponding jump process (22, 23),

$$\frac{\partial P_G(f,t)}{\partial t} = \int \mathrm{d}f' \underbrace{\phi_G^{\mathcal{T}}(f,f')\rho(f,f')\mu}_{T_{f\leftarrow f'}} P_G(f',t) - \int \mathrm{d}f' \underbrace{\phi_G^{\mathcal{T}}(f',f)\rho(f',f)\mu}_{T_{f'\leftarrow f}} P_G(f,t), \quad [2]$$

where $T_{f'\leftarrow f}$ is the probability to change the population's fitness from f to f'. $T_{f'\leftarrow f}$ is given by the product of the probability of mutation, μ, the probability that a mutant with fitness f' arises, $\rho(f',f)$, and the probability that such a mutation, arising preferentially in nodes that are replaced often, reaches fixation, $\phi_G^{\mathcal{T}}(f',f)$ (where $\mathcal{T}$ denotes temperature initialization). The probability $T_{f\leftarrow f'}$ is given by an equivalent argument.

The reason behind using fixation probability under temperature initialization is that the probability for a mutant to arise on a certain node during reproduction in a homogenous population is proportional to the temperature of that node (20). This follows from our assumption that during a birth event, it is always the offspring individual that replaces a neighboring individual. For the opposite case, where the parent individual replaces a neighboring individual and the offspring (potentially a mutant) individual stays at the focal node, the fixation probability for uniform initialization has to be used in Eq. **2** instead. The corresponding evolutionary dynamics on the fitness space is a biased random walk with transition rates $T_{f'\leftarrow f}$ and $T_{f\leftarrow f'}$. To derive the steady state, $P_G^*(f)$, we start from the assumption of detailed balance (23),

$$\int \mathrm{d}f' \; T_{f\leftarrow f'} P_G^*(f') = \int \mathrm{d}f' \; T_{f'\leftarrow f} P_G^*(f). \qquad [3]$$

This condition is fulfilled if we have $T_{f\leftarrow f'} P_G^*(f') = T_{f'\leftarrow f} P_G^*(f)$ for all f, f'. From this, we obtain the steady state (23),

$$P_G^*(f) = \frac{1}{\int \mathrm{d}f' \, \frac{T_{f'\leftarrow f}}{T_{f\leftarrow f'}}} = \frac{1}{\int \mathrm{d}f' \, \frac{\phi_G^{\mathcal{T}}(f',f)}{\phi_G^{\mathcal{T}}(f,f')} \cdot \frac{\rho(f',f)}{\rho(f,f')}}. \qquad [4]$$

If the mutant's fitness distribution $\rho(f',f)$ only depends on the fitness distance between parent and offspring, $\rho(f',f) = \rho(|f'-f|)$, the population's steady-state statistics depends only on the fixation probabilities—in this case, the second factor cancels out. Furthermore, the steady-state probability density for the population's fitness is the same for all isothermal graphs, irrespective of the offspring mutational fitness distribution—the first factor is the same for all isothermal graphs, including the complete graph.

As an example, the steady-state distribution for the complete graph when mutant's fitness is sampled from the uniform distribution is

$$P_C^*(f) = \frac{N}{f_{\max}^N - f_{\min}^N} f^{N-1}. \qquad [5]$$

See *App. A* for details. This steady-state statistics is exactly the same as derived in ref. 24. However, in ref. 24, the evolutionary dynamics was studied by using a nearest-neighbor jump process on a discretized state space. In our derivation of Eq. **5**, at a given point in the dynamics, the population could jump to any arbitrary point of the fitness space. Yet, interestingly, we obtain the same steady-state distribution for the complete graph as derived in ref. 24, but for a different scenario.

To study mutation–selection balance on graphs, we choose the complete graph, the star graph, and the (weighted) star graph with self-loops, i.e., a star where every individual can also be replaced by its own offspring. Under temperature initialization, a complete graph is an isothermal graph. For finite N, the star is a suppressor of fixation (for $N \to \infty$, it becomes a suppressor of selection), and the star graph with self-loops is a piece-wise amplifier of selection (20) (only for $N \to \infty$, it becomes an amplifier in a strict sense) (Fig. 2 *B* and *D*). Adding self-loops and making edges weighted can make the star graph an amplifier of selection for temperature initialization. According to ref. 25, for a structure to be an amplifier of selection, it should have a sufficient number of cold nodes (low-temperature nodes), where a mutant is less likely to get replaced by wild-type individuals and, thus, increasing the likelihood for a mutant to fix. The star graph (unweighted, without self-loops) indeed has many cold nodes, making it an amplifier of selection under uniform initialization (1) (Fig. 2 *A* and *C*). However, under the temperature initialization process, the initial mutant appears on the central node with high probability, as the central node has the highest temperature. Thus, the mutant is more likely to get extinct during the course of the dynamics, explaining its suppressing nature. By adding self-loops to the star graph with a larger weight, one decreases the temperature of the central node and increases the temperature of the leaves, thus increasing the likelihood for the leaf nodes to receive an initial mutant. This transformation facilitated via self-loops and weighted edges is the reason behind the amplifying nature of the self-looped star graph.

We use these graphs because exact expressions for the corresponding fixation probabilities are known (*App. C*). The fixation probabilities for these three graphs under uniform and temperature initialization are plotted as a function of the mutant's fitness in Fig. 2.

The microscopic Moran-Bd update is costly to simulate for low mutation rates, especially for large graphs. Thus, we use a coarse-grained description, where we focus on the changes arising from mutations. We use the following Monte Carlo-type algorithm (26, 27), which measures time steps in terms of mutational events:

- An initial fitness value f between $f_{\min}$ and $f_{\max}$ is assigned to each individual in a population on a graph G.
- At every time step, a mutant f' is drawn from a distribution $\rho(f',f)$.
- The fitness of the entire population is then updated to f' with probability $\phi_G^{\mathcal{T}}(f',f)$. With probability $1-\phi_G^{\mathcal{T}}(f',f)$, it remains the same. Note that this step takes into account that mutants tend to arise in different places with different probabilities.
- The last two steps are repeated for a sufficiently long number of time steps until a mutation–selection balance is attained.

We use this algorithm to infer how mutation–selection balance is attained in our three spatial structures. In Fig. 3 *A* and *B*, the independent fitness trajectories, as well as the ensemble average fitness trajectory of the population, are plotted as a function of the number of mutations occurred.

Results

The star with self-loops, an amplifier of selection, reaches the highest steady-state fitness in its mutation–selection balance (Fig. 3*B*). This is expected because, compared to the other graphs, the self-looped star graph is best at fixing beneficial mutants for temperature initialization. What is surprising is that the star graph, a suppressor of fixation with lower fixation probability for all fitness values of a mutant, attains not just higher steady-state fitness than the complete graph (and, thus, all isothermal graphs), but almost the same balance as the star with loops, an amplifier of selection. We also observe that, just like isothermal networks, the star graph with loops takes fewer mutations to reach the balance than the star graphs, which takes many more mutations to reach the steady

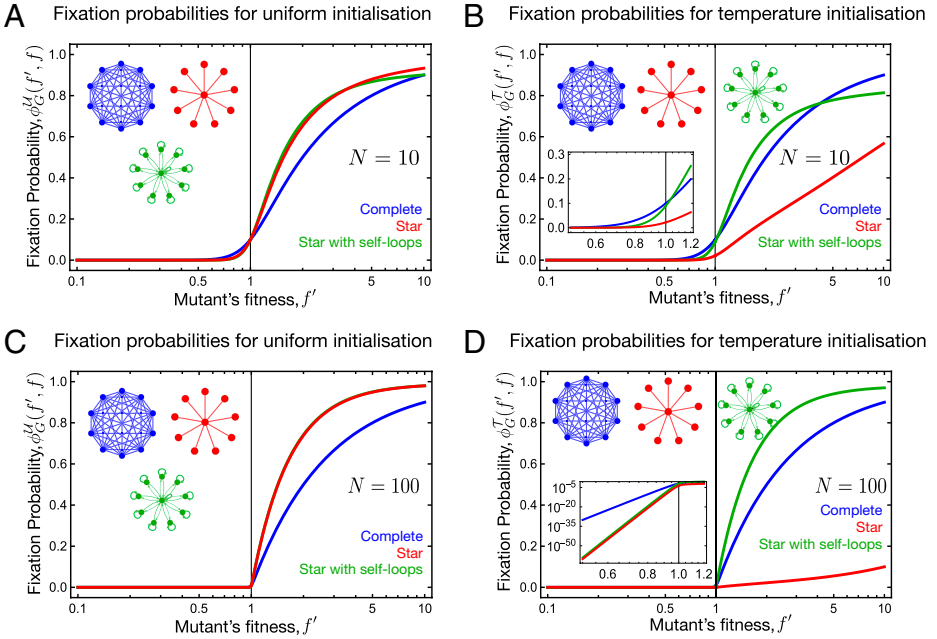

Fig. 2. Fixation probabilities for uniform and temperature initialization. (*A*) The fixation probabilities $\phi_G^{\mathcal{U}}(f', f)$ as functions of mutant's fitness f' with background fitness $f = 1$ for uniform initialization $\mathcal{U}$ for three graphs with $N = 10$: the complete graph, the star, and a weighted star with self-loops. For this initialization scheme, both the star and the star with loops are amplifiers of selection, and all fixation probabilities intersect at $f' = f$ and $\phi_G^{\mathcal{U}}(f, f) = N^{-1}$. (*B*) Fixation probabilities as in *A*, but for temperature initialization. Now, the star with self-loops is only a piecewise amplifier of selection, as it reduces the fixation probability for very large f'. The star is a suppressor of fixation and reduces the fixation probability for all mutant fitness values. Note that even under neutrality, $f' = 1$, the fixation probabilities are different. (*C*) Fixation probabilities as in *A*, but with $N = 100$. For large N, probabilities to fix deleterious mutants decrease, while they increase for the beneficial mutants. (*D*) For temperature initialization, a larger self-looped star graph amplifies selection for the entire fitness domain considered in the figure. On the other hand, even at $N = 100$, the star graph continues to be a suppressor of fixation; see *D*, *Inset* (Parameters: with n leaves, the weight of all the leaves' self-loops is $1 - n^{-1}$, and the weight for the center's self-loop is $1 - n^{-2}$. All the links directed from the center to leaves and vice versa have weights n^{-3} and n^{-1}, respectively.

state. In the subsequent sections, we will discuss these observations and give an explanation for them.

Amplifiers Attain Higher Steady-State Fitness in Mutation–Selection Equilibrium. Amplifiers of selection are better at fixing beneficial mutants and avoiding the fixation of deleterious mutants than isothermal graphs. They are expected to attain a higher steady-state fitness in the mutation–selection balance than isothermal graphs. We verify this expectation in Fig. 3 *C* and *D*, which shows the average steady-state fitness of the population for different population sizes. We consider two types of mutational fitness jump distribution, a uniform and a (truncated) Gaussian, centered around the parent's fitness. We observe that, regardless of the mutational fitness distribution, the star graph with loops attains a higher steady-state fitness than the complete graph for all considered population sizes. In *App. B*, we provide a formal proof that, for any mutational fitness distributions, amplifiers of selection have higher steady-state fitness than well-mixed populations and suppressors of selection. As a reference, by using Eq. **5**, we derive the steady-state average fitness for the complete graph with uniform mutational fitness distribution,

$$\langle f \rangle_C^* = \frac{N}{N+1} \frac{f_{\max}^{N+1} - f_{\min}^{N+1}}{f_{\max}^{N} - f_{\min}^{N}}. \qquad [6]$$

Thus, in the limit of large N, $\langle f \rangle_C^* \to f_{\max}$. The steady-state fitness approaches the maximal possible value, $\langle f \rangle^* \to f_{\max}$ for $N \to \infty$, for both the complete and the self-looped star graph. This is true for a general mutational fitness distribution, where there is always a finite probability to fix a beneficial mutation, and where the probability to fix a deleterious mutant goes to zero in the limit of $N \to \infty$. In fact, $f_{\max}$ becomes an absorbing state for the evolutionary trajectories on the amplifiers of selection and the well-mixed population. Therefore, the fluctuations around the steady state for these graphs also go to zero. This can be illustrated by studying the large-N limit dynamics of the self-looped star graph and the complete graph. In the limit of $N \to \infty$, the fixation probability for the self-looped star under temperature initialization becomes $1 - f^2/f'^2$ for any $f' > f$ and 0 otherwise (*App. C*), whereas from Eq. **1**, it follows that for the complete graph, the fixation probability becomes, $1 - f/f'$ for $f' > f$ and 0 otherwise. Hence, in the limit of $N \to \infty$, both of these graphs can only fix beneficial mutants, and, thus, the long-term mutation–selection dynamics gets absorbed at $f_{\max}$. This also leads to the conclusion that the self-looped star needs fewer mutations than the complete graph to reach $f_{\max}$. The large-N analysis for the star graph (unweighted and without self-loops), however, is a bit subtle, as in the limit of $N \to \infty$, the fixation probability becomes zero for all possible pairs of mutant and background fitness values. For very large, but finite, *App. D*, we show that the steady-state average fitness for the star graph also converges to $f_{\max}$.

Do Amplifiers Maximize Average Fitness? The star graph with no self-loops, a suppressor of fixation, not only attains higher steady-state fitness in the mutation–selection balance than the complete graph, but almost the same steady-state fitness as the star with self-loops, an amplifier of selection, as shown in Fig. 3 *C* and *D*. In *App. D*, we show that even for very large N, the star graph continues to attain higher steady-state average fitness than the well-mixed population. There are two main factors that drive the steady-state fitness: 1) fixing beneficial mutants with high probability and 2) avoiding the fixation of deleterious mutants. As an amplifier of selection, the star with self-loops is superior in fixing beneficial mutants. But the star without self-loops is much better at avoiding the fixation of deleterious mutants (Fig. 2 *B*, *Inset*, and *D*, *Inset*). In this way, the star without self-loops

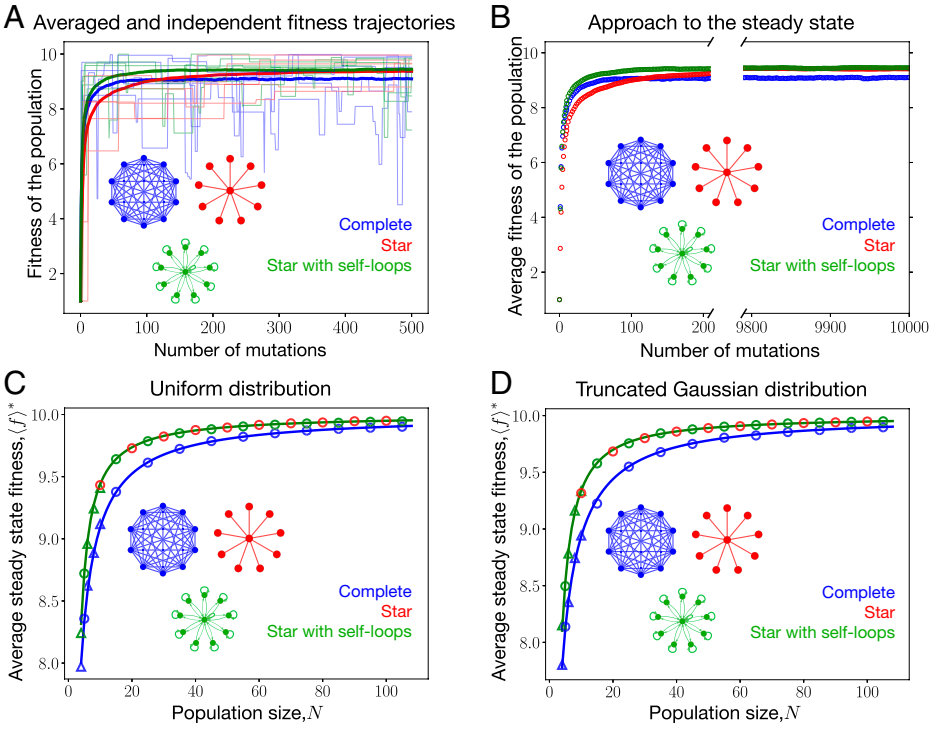

Fig. 3. Fitness trajectories and steady-state average fitness for different graphs. (*A*) The average fitness trajectories (in dark colors) for the complete graph, the star graph, and the self-looped star graph with a uniform mutational fitness distribution, starting from a population where every individual has fitness $f = 1$. For each graph, the average fitness trajectory is computed by performing an ensemble average over an ensemble of 2,000 independent realizations. In the background of *A*, five such independent realizations are shown (in light colors) for each graph. After reaching high fitness value, the fitness of the complete graphed population fluctuates more than the other two graphs. This is because after reaching higher fitness values, deleterious mutations become more likely to appear. The complete graph is worse at rejecting such deleterious mutants compared to other two graphs (Fig. 2 *B*, *Inset*, and *D*, *Inset*); it experiences more fluctuations. (*B*) Although the star is a suppressor of fixation, it attains the same steady-state fitness in the mutation–selection balance as the self-looped star graph. This is due to its better response to deleterious mutants (Fig. 2 *B*, *Inset*, and *D*, *Inset*). In *C* and *D*, steady-state fitnesses in the mutation–selection balance attained for the self-looped star graph (green) and complete graph (blue) as a function of population size are shown in with uniform (*C*) and truncated (*D*) Gaussian mutational fitness distribution. The SD for the Gaussian distribution is chosen to be $\sigma = 1$. Solid lines are the numerical solutions of Eq. **4**, and circles represent simulation points obtained using the Monte Carlo algorithm, while triangles correspond to microscopic Moran Bd simulations, which are feasible only for very small *N*. Regardless of the mutational fitness distribution, the self-looped star (an amplifier) always attains higher steady-state fitness in the mutation–selection balance than isothermal graphs for all (finite) *N*. Red circles correspond to the steady-state fitness attained by the star graph, a suppressor of fixation. From *C* and *D*, we find that even for large *N*, the star graph reaches almost the same steady-state fitness as that of the self-looped star graph. Parameters $N = 10$, $f_{\text{min}} = 0.1$, and $f_{\text{max}} = 10$.

compensates for its lower fixation probabilities of beneficial mutants. Therefore, the fixation probability profile for deleterious mutants can contribute considerably to the long-term mutation–selection evolutionary dynamics. We expect this to be quite general, and not just restricted to the graphs that we have considered. We argue this in the following way: Let us take two amplifiers, A_1 and A_2, and, without any loss of generality, assume that A_1 is a better amplifier than A_2. That is, A_1 is better in fixing advantageous mutants and avoiding the fixation of deleterious mutants than A_2. In that case, by the proof given in *App. B*, it follows that the average steady-state fitness of A_1 is greater than the average steady-state fitness of A_2—i.e., $\langle f \rangle^*_{A_1} > \langle f \rangle^*_{A_2}$. However, if A_2 can be modified, along the lines of ref. 28, such that its fixation probability for deleterious mutants becomes much lower than A_1, the average steady-state fitness $\langle f \rangle^*_{A_2}$ can exceed $\langle f \rangle^*_{A_1}$. But this compensation for lower fixation probabilities of beneficial mutants by decreasing the acceptance rate of deleterious mutants comes at a cost in terms of the time it takes to reach the steady state.

Time to Reach the Steady State. So far, we have studied the steady-state average fitness values for different graphs. Now, we discuss the time they take to reach their respective steady states. To estimate these times, we use the concept of mixing times (29). In a generic stochastic process, the probability distribution $P_G(f)$ defined on a space Ω changes with time before reaching its steady state. The mixing time can then be defined as the time when the distance of this evolving distribution to its steady state $P^*_G(f)$ goes to zero. Formally, the mixing time t_{mix} is defined as the minimal time when the distance $d(t)$ to the steady-state distribution is smaller than a threshold ε,

$$t_{\text{mix}}(\varepsilon) = \min\{t : d(t) \leq \varepsilon\}, \qquad [7]$$

where

$$d(t) = \frac{1}{2} \sum_{f \in \Omega} |P_G(f, t) - P^*_G(f)|. \qquad [8]$$

In Fig. 4*A*, we find that the star graph, a suppressor of fixation, attains the same balance as the self-looped star, but takes many more mutations to reach the steady state than all other considered graphs. The mixing times for the complete and the self-looped star do not vary much with the population size. In fact, it decreases for the self-looped star with increasing N. This is because the self-looped star becomes a better amplifier for larger N (Fig. 2 *B* and *D*). Adaptation for the complete graph and the self-looped star graph is mostly governed by the fixation of beneficial mutants, which improves with large N. On the other hand, the adaptation for the star graph depends crucially on preventing the fixation of deleterious mutants, as it becomes less likely to

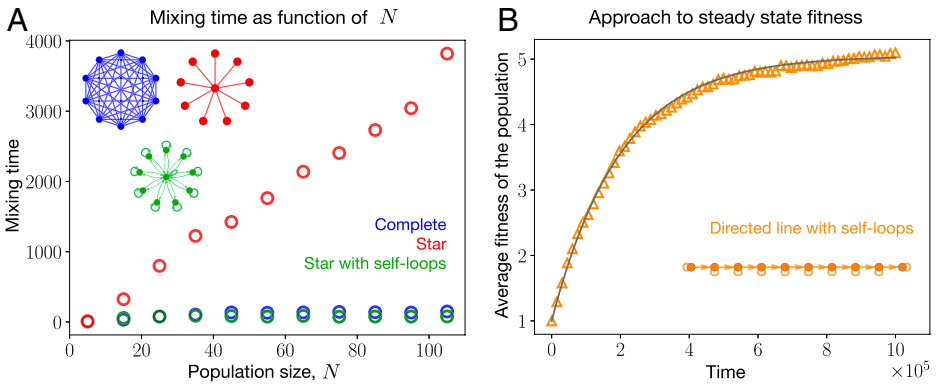

Fig. 4. Approach to the steady state. (*A*) Mixing time for various graphs as a function of population size *N* measured in number of mutations. Parameters are same as in Fig. 3*C*. Mixing times have been obtained by using the Monte Carlo algorithm. The star graph takes the longest to reach a steady state. This is because the star graph, especially for large *N*, has very small fixation probabilities, even for beneficial mutants, and, thus, more attempts to increase fitness are needed to reach the steady state (for the mixing time, we assume $\varepsilon = \frac{1}{4}$ in Eq. **7**). (*B*) Increase of average fitness on the directed line with self-loops. We compare Eq. **42** and the corresponding microscopic Moran Bd simulations. Parameters are the same as in Fig. 3, with a mutation probability $\mu = 10^{-4}$. We see a good agreement between simulations (orange symbols) and the analytical result (gray line). From *App. E*, we know that the relaxation time for single rooted graphs goes as $\frac{N}{\mu \mathcal{T}_r}$. Substituting values for the parameters and the root temperature for the directed line with self-loops, $\mathcal{T}_r = \frac{1}{2}$, we get the mixing time to be approximately 2×10^5. Here, the time is measured in terms of the number of Moran Bd steps. Although the simulation here is performed for the self-looped directed line, the same result is expected for any other single rooted (self-looped) graph, as long as μ is sufficiently low. For more details, see *App. E*.

fix beneficial mutants with the increase in N (Fig. 2 *B* and *D*). Therefore, most mutations arising in this graph do not reach fixation. Another interesting observation is that for large N, the self-looped star graph has the smallest mixing time. This contrasts with the typical fixation probability and time relation, where larger fixation probability tends to correlate with higher fixation times (30–33). The mixing time is difficult to calculate for the general case. But for single rooted graphs with $\phi_G^{\mathcal{T}} \sim \frac{1}{N}$, it can be computed efficiently. In fact, for single rooted graphs, the full temporal statistics can be computed (*App. E*). In Fig. 4*B*, we see a good agreement between the microscopic Moran Bd simulations performed for the self-looped directed line and the analytical expression for the average fitness trajectory (Eq. **42**). We also verify that the self-looped directed line, a suppressor of selection, attains lower steady-state average fitness in the mutation–selection balance than the complete graph and the self-looped star graph. This is in accordance with *App. B*, where suppressors of selection are proved to attain lower steady-state fitness than the complete graph and amplifiers of selection.

Gaussian Phenotype-Fitness Map. Until now, the dynamics were considered in fitness space. However, in many cases, mutations occur on the level of an individual's phenotype. In that case, the state of a population is represented by a phenotype vector $\mathbf{p} = (p_1, p_2, \cdots, p_{N-1}, p_N)^{\mathrm{T}}$, where p_i is the phenotypic trait value of the individual at node i. The Moran Bd update still only takes the fitness of individuals into account. Therefore, a phenotype-fitness map $f(p)$ is used to assign a fitness value to a phenotype. The fitness profile of the population can then be denoted by $\mathbf{f}(\mathbf{p}) = (f(p_1), f(p_2), \cdots, f(p_N))^{\mathrm{T}}$. Similar to the previous case, when an offspring is mutated, we choose its phenotype p' from a continuous bounded distribution $\rho(p', p)$, where p is the parent's phenotypic value and $p_{\min} \leq p' \leq p_{\max}$. In this way, the work presented so far is identical to what would be obtained by considering a linear phenotype-fitness map, $f(p) = p$. In this section, we study the dynamics of a nonmonotonic Gaussian phenotype-fitness map. In Fig. 5*A*, we show that the order of the steady-state fitness in mutation–selection balance for different graphs remains the same as that of the linear phenotype-fitness

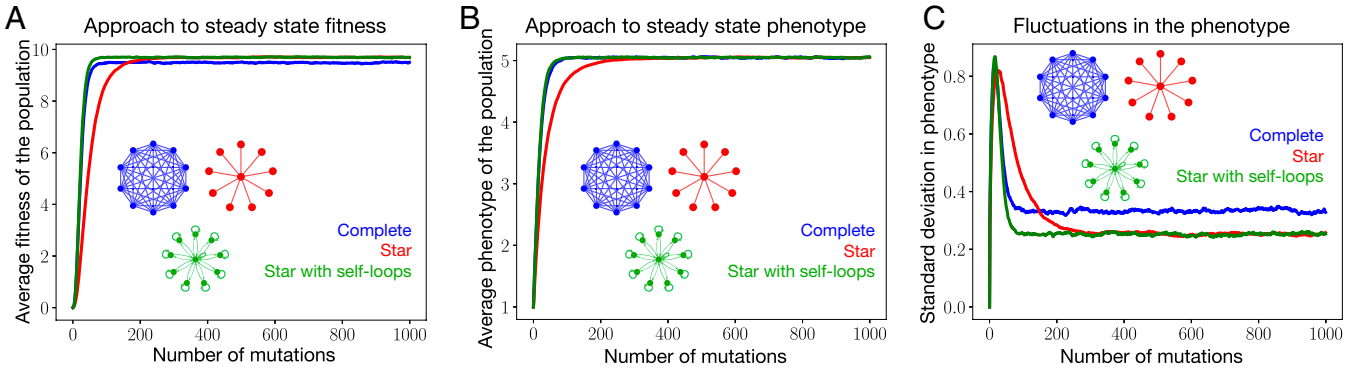

Fig. 5. Gaussian phenotype-fitness map: Fitness and phenotypic trajectories for different graphs. Here, we consider a Gaussian phenotype-fitness map, $f(p) = f_{\mathrm{opt}} \exp(-\frac{(p-p_{\mathrm{opt}})^2}{2\sigma_p^2})$, where p_{opt} is the optimal phenotype, where the fitness is maximal and $f(p_{\mathrm{opt}}) = f_{\mathrm{opt}}$. (*A*) As in the case of a linear phenotype-fitness map, the star and the self-looped star have a higher state fitness than isothermal graphs. (*B*) All graphs converge to an average phenotype corresponding to the fitness maximum, but they have different fitness in steady state (*A*). The reason for this is differences in the fluctuations in steady state. (*C*) The SD of the phenotypes shows that the complete graph is more prone to fluctuations than the other two graphs. Parameters $f_{\mathrm{opt}} = 10$, $p_{\mathrm{opt}} = 5.05$, and $\sigma_p = 1$, all other parameters are as in the previous figures, with $\sigma = 0.5$ for the Gaussian mutational jump phenotype distribution.

map. It is interesting to note that the average steady-state phenotype for all the graphs is the same (Fig. 5*B*). Nevertheless, we see different steady-state average fitness values. Even though all graphs have the same steady-state phenotypic value, isothermal graphs are more prone to fluctuations and have a lower steady-state average fitness value (Fig. 5*C*). This happens again because the other two graphs are better in preventing the fixation of deleterious mutants. At long times, after reaching higher fitness values, populations are more likely to receive deleterious mutations than beneficial ones. Therefore, in the steady state, what determines fitness fluctuations of a population is its ability to reject deleterious mutants. In a nutshell, the steady-state fitnesses of graphs need not be same even when they have same phenotypes because the average of a function in general is not equal to the function of average, i.e., $\langle f(p)\rangle \neq f(\langle p\rangle)$.

Discussion

In evolutionary graph theory, evolutionary dynamics on graph structures has been studied in great detail. While the field has been mostly driven from the mathematical and computational community (1, 2, 19, 25, 32), partly driven by biological applications (17, 34, 35), now, there is increasing interest in applying these ideas to experimental systems in microbiology (36, 37).

The prospects of engineering a population structure that can optimize the chances to evolve certain mutations or to observe evolved population structures that minimize the evolution of mutations seem exciting, but these applications call for an extension of the field of evolutionary graph theory: Most applications implicitly assume that each node is a small population, and not all results carry over from graphs of individuals to graphs of subpopulations (38–41). In addition, the field has focused so far on fixation probability and fixation time (42–49).

This approach assumes that we can focus on the fate of a single mutant, but it can break down when mutations continuously arise, especially in graphs where the time to fixation or extinction is very high. Moreover, in the case where mutations continuously arise, one has to take into account where they arise. Thus, one needs to work with temperature initialization, where the definitions of amplifiers and suppressors of selection are less clear-cut.

We developed a model that takes such a continuous supply of mutations into account. We worked in the low mutation rate regime, where the fixation time of a mutant is much smaller than the average time between the two successive mutants. We found that the prevention of deleterious mutants from fixing can be more important than increasing the chances of advantageous mutants in order to obtain a higher steady-state fitness in the mutation–selection balance. In our case, the star, a suppressor of fixation for temperature initialization, beats isothermal graphs and attains almost the same balance as a self-looped star, an amplifier. The cause for this is the ability of the star graph to prevent deleterious mutants much better from fixing than isothermal graphs. The deleterious mutants regime is usually overlooked in the literature while studying fixation probabilities by using large-N arguments. However, here, we have shown that the deleterious mutants regime is equally important, if not more, even for large N, as the beneficial mutants regime when studying long-term evolutionary dynamics.

Typically, amplifiers of selection also have a higher fixation time (25, 32, 33). Thus, one has to be careful that the assumption of small mutation rate is still fulfilled. When the fixation time becomes comparable to the average time between two successive mutations, one expects deviation from the low mutation rate approximation. On going beyond the weak mutation approximation, we found that the star continues to maintain higher steady-state average fitness in the mutation–selection balance than the complete graph, while the self-looped star attains a lower steady-state average fitness than the complete graph outside the low mutation rate (*App. F*). Therefore, an amplifier of selection need not maximize fitness both inside and outside the low mutation rate regime. However, within the weak mutation rate regime, structures that allow more mutations to reach fixation will have a smaller mixing time—therefore, amplifiers of selection tend to have a lower mixing time until their steady-state fitness is reached.

Due to their ability to reach a high steady-state fitness, population structures that suppress selection could be much more interesting in applications than previously thought—suppressing selection may be as relevant as amplifying it. We have shown that in a situation where a dynamic, graph-structured population continuously evolves, the amplification of selection via the promotion of advantageous mutations does not necessarily imply a higher steady-state fitness. Instead, in such a process, one has to carefully consider also the fate of deleterious mutations, an issue that has so far not been in the focus of evolutionary graph theory.

Appendix

A. Steady State for the Complete Graph. Here, we derive the mutation-selection balance steady-state statistics for the complete graph. To do so, we assume that the mutant's fitness is drawn from a uniform distribution defined over the domain $[f_{\min}, f_{\max}]$. Therefore, the general form of the steady-state fitness distribution, Eq. **4**, reduces to

$$P^*_G(f) = \frac{1}{\int \mathrm{d}f' \, \frac{\phi^{\mathcal{T}}_G(f',f)}{\phi^{\mathcal{T}}_G(f,f')} \cdot 1}. \qquad [9]$$

By inserting the fixation probabilities for the complete graph in the above equation using Eq. **1**, we obtain

$$P^*_C(f) = \frac{1}{\int \mathrm{d}f' \, \left(\frac{f'}{f}\right)^{N-1}} = \frac{f^{N-1}}{\int \mathrm{d}f' \, f'^{N-1}} = \frac{N f^{N-1}}{f^N_{\max} - f^N_{\min}}. \qquad [10]$$

Using the above distribution, the steady-state average fitness in the mutation–selection balance for the complete graph takes the form,

$$\langle f\rangle^*_C = \int \mathrm{d}f \; f P^*_C(f) = \frac{N}{N+1} \frac{f^{N+1}_{\max} - f^{N+1}_{\min}}{f^N_{\max} - f^N_{\min}}. \qquad [11]$$

B. Amplifiers of Selection Attain Higher Steady-State Fitness in Mutation–Selection Balance than Suppressors of Selection. Here, we prove that amplifiers of selection attain higher steady-state fitness in their mutation–selection balance than suppressors of selection. We denote an arbitrary amplifier by A and an arbitrary suppressor by S. From the definitions of amplifiers and suppressors mentioned in the introduction, we have for every $f' < f$ (and arbitrary initialization scheme $\mathcal{I}$)

$$\phi^{\mathcal{I}}_A(f,f') > \phi^{\mathcal{I}}_S(f,f'), \qquad [12]$$

as well as

$$\phi^{\mathcal{I}}_A(f',f) < \phi^{\mathcal{I}}_S(f',f), \qquad [13]$$

Combining these two inequalities, we get,

$$\frac{\phi^{\mathcal{I}}_A(f',f)}{\phi^{\mathcal{I}}_A(f,f')} < \frac{\phi^{\mathcal{I}}_S(f',f)}{\phi^{\mathcal{I}}_S(f,f')}. \qquad [14]$$

Multiplying the above equation with $\rho(f',f)/\rho(f,f')$, followed by integrating over f' from $f_{\min}$ to f, we obtain,

$$\int_{f_{\min}}^{f} \mathrm{d}f' \, \frac{\phi_A^{\mathcal{I}}(f',f)}{\phi_A^{\mathcal{I}}(f,f')} \cdot \frac{\rho(f',f)}{\rho(f,f')} < \int_{f_{\min}}^{f} \mathrm{d}f' \, \frac{\phi_S^{\mathcal{I}}(f',f)}{\phi_S^{\mathcal{I}}(f,f')} \cdot \frac{\rho(f',f)}{\rho(f,f')}. \quad [15]$$

Similarly, we find,

$$\int_{f}^{f_{\max}} \mathrm{d}f' \, \frac{\phi_A^{\mathcal{I}}(f',f)}{\phi_A^{\mathcal{I}}(f,f')} \cdot \frac{\rho(f',f)}{\rho(f,f')} > \int_{f}^{f_{\max}} \mathrm{d}f' \, \frac{\phi_S^{\mathcal{I}}(f',f)}{\phi_S^{\mathcal{I}}(f,f')} \cdot \frac{\rho(f',f)}{\rho(f,f')}. \quad [16]$$

By making use of the steady-state solution Eqs. **4** and **15**, we find an inequality for probability density functions at the boundary $f_{\max}$ of the fitness domain,

$$P_A^*(f_{\max}) > P_S^*(f_{\max}). \quad [17]$$

While Eq. **4** contains temperature-initialized fixation probabilities, the same expression follows for the steady-state statistics for any arbitrary initialization. As an example, instead of the mutations taking place during reproduction, they could appear spontaneously at any of the nodes. Eq. **4** would then contain uniform initialized fixation probabilities.

Similarly, at the fitness boundary $f_{\min}$, using Eqs. **4** and **16**, we have,

$$P_A^*(f_{\min}) < P_S^*(f_{\min}). \quad [18]$$

The very same inequalities, [**17**] and [**18**], hold if A (amplifier) or S (suppressor) is replaced by C (complete).

Let us now first prove that amplifiers of selection attain higher steady-state fitness in mutation–selection balance than the complete graph. We take the case of an amplifier and the complete graph of the same size. The inequalities [**17**] and [**18**] imply that there exists a fitness, $\hat{f}$, such that,

$$P_A^*(\hat{f}) = P_C^*(\hat{f}). \quad [19]$$

For simplicity, here, we assumed that there is only one intersection point for the curves $P_A^*(f)$ and $P_C^*(f)$. The proof, however, is not restricted to this assumption and can be extended to the general case where more than one intersection points are there. The main idea behind the proof is sketched in Fig. 6.

Let us define the $P_A^*(f)$ as:

$$P_A^*(f) = \begin{cases} P_C^*(f) + \varepsilon_A^<(f), & \text{if } f \le \hat{f} \\ P_C^*(f) + \varepsilon_A^>(f), & \text{otherwise.} \end{cases} \quad [20]$$

From the normalization condition of $P_A^*(f)$ and $P_C^*(f)$, it follows that

$$\left| \int_{f_{\min}}^{\hat{f}} \mathrm{d}f \, \varepsilon_A^<(f) \right| = \int_{\hat{f}}^{f_{\max}} \mathrm{d}f \, \varepsilon_A^>(f). \quad [21]$$

We are interested in the difference of mean fitness in the steady state,

$$\langle f \rangle_A^* - \langle f \rangle_C^* = \underbrace{\int_{f_{\min}}^{\hat{f}} \mathrm{d}f \, f \varepsilon_A^<(f)}_{\Gamma_1} + \underbrace{\int_{\hat{f}}^{f_{\max}} \mathrm{d}f \, f \varepsilon_A^>(f)}_{\Gamma_2}. \quad [22]$$

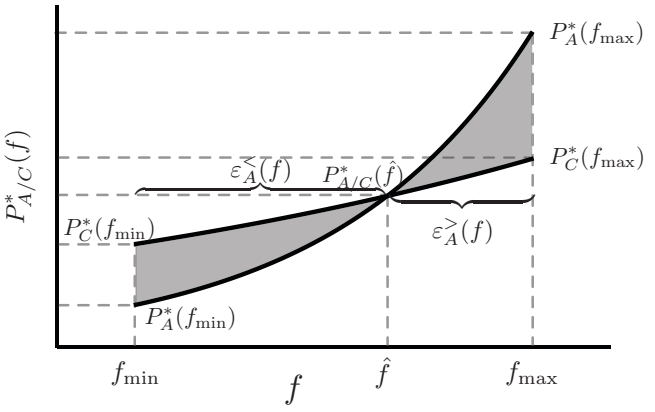

Fig. 6. Sketch for the proof. Here, we sketch the main idea behind the proof that the average fitness of an amplifier of selection exceeds that of a suppressor of selection or the complete graph in the steady state. Without any loss of generality, we take the case of an amplifier *A* and the complete graph *C*. The proof starts by first computing the order of $P_{A/C}^*(f)$ at the fitness boundaries $f_{\min}$ and $f_{\max}$. It turns out that $P_A^*(f_{\min}) < P_C^*(f_{\min})$ and $P_A^*(f_{\max}) > P_C^*(f_{\max})$. This implies that there exists a fitness point $\hat{f}$, where these probability densities intersect. P_A^* is then decomposed as the sum of P_C^* and the functions $\varepsilon_A^{</>}$ (Eq. **20**). By using the normalization conditions for P_C^* and the properties of functions $\varepsilon_A^{</>}$ (Eq. **21**), we prove that amplifiers of selection attain higher steady-state fitness than the well-mixed population and, by extension, the suppressors of selection.

The first term in the above equation is negative, $\Gamma_1 < 0$, while the second term is positive, $\Gamma_2 > 0$. In the following, we show that the magnitude of the term Γ_1 is less than the term Γ_2. Taking Γ_1, we find that

$$|\Gamma_1| < \hat{f} \left| \int_{f_{\min}}^{\hat{f}} \mathrm{d}f \, \varepsilon_A^<(f) \right|. \quad [23]$$

Similarly,

$$\hat{f} \int_{\hat{f}}^{f_{\max}} \mathrm{d}f \, \varepsilon_A^>(f) < \Gamma_2. \quad [24]$$

Now, because

$$\hat{f} \left| \int_{f_{\min}}^{\hat{f}} \mathrm{d}f \, \varepsilon_A^<(f) \right| = \hat{f} \int_{\hat{f}}^{f_{\max}} \mathrm{d}f \, \varepsilon_A^>(f), \quad [25]$$

using inequalities [**23**] and [**24**], we find $|\Gamma_1| < \Gamma_2$. Therefore, at last, we have

$$\langle f \rangle_A^* > \langle f \rangle_C^*. \quad [26]$$

Following the same procedure, one can show that $\langle f \rangle_C^* > \langle f \rangle_S^*$. This implies that $\langle f \rangle_A^* > \langle f \rangle_S^*$ for all amplifiers of selection A and suppressors of selection S.

C. Fixation Probability for the Weighted Self-Looped Star Graph under Temperature Initialization. In this section, we introduce the weighted self-looped star graph that has been used throughout the main text. It is defined by the weighted adjacency matrix

$$\mathbf{w} = \begin{pmatrix} 1-\delta & \frac{\delta}{n} & \frac{\delta}{n} & \cdots & \frac{\delta}{n} \\ \lambda & 1-\lambda & 0 & \cdots & 0 \\ \vdots & \vdots & \ddots & \ddots & \vdots \\ \lambda & 0 & \cdots & 1-\lambda & 0 \\ \lambda & 0 & \cdots & 0 & 1-\lambda \end{pmatrix}, \quad [27]$$

with $0<\lambda\leq 1$ and $0<\delta\leq 1$. Here, w_{ij} is the weight of the link directed from the node i to node j, with the center being the node 0. The fixation probability under temperature initialization for this graph has been derived by using the techniques of martingales (3, 20) and is given by

$$\phi^{\mathcal{T}}_{G_{n+1}(\lambda,\delta)}(f',f)=\frac{1-\left(\frac{f'}{f}\right)^2}{n\lambda\frac{f'}{f}+\delta}\frac{1}{n+1}\times\frac{n^3(1-\lambda)\lambda^2+n^2\lambda\delta\left(\frac{f'}{f}+\lambda\right)+n\lambda\delta\left(\frac{f'}{f}+\delta\right)+(1-\delta)\delta^2}{\left(n\lambda\frac{f'}{f}+\delta\right)\left(\frac{\delta\frac{f'}{f}+n\lambda}{\delta\frac{f'}{f}+n\lambda\left(\frac{f'}{f}\right)^2}\right)^n-\frac{f'}{f}\left(\delta\frac{f'}{f}+n\lambda\right)}, \quad [28]$$

where $G_{n+1}(\lambda,\delta)$ denotes the weighted self-looped star graph with n leaves. In the limit of $n\to\infty$, when λ and δ are independent of n, Eq. **28** becomes,

$$\lim_{n\to\infty}\phi^{\mathcal{T}}_{G_{n+1}(\lambda,\delta)}(f',f)=\begin{cases}\left(1-\left(\frac{f}{f'}\right)^2\right)(1-\lambda), & \text{if } f'>f,\\ 0 & \text{otherwise.}\end{cases} \quad [29]$$

We use two versions of this weighted graph by first setting $\lambda=\delta=1$ in the above equation that results in the unweighted star graph, which, however, is a suppressor in the limit $n\to\infty$ under temperature initialization. This is reflected by $\lim_{n\to\infty}\phi^{\mathcal{T}}_{G_{n+1}(\lambda=1,\delta=1)}(f',f)=0$ for all f' and f. Setting instead $\lambda=\frac{1}{n}$ and $\delta=\frac{1}{n^2}$ followed by taking the infinite population size limit of Eq. **28** yields a structure that is an amplifier for $n\to\infty$. That is,

$$\lim_{n\to\infty}\phi^{\mathcal{T}}_{G_{n+1}(\lambda,\delta)}(f',f)=\begin{cases}1-\left(\frac{f}{f'}\right)^2, & \text{if } f'>f,\\ 0 & \text{otherwise.}\end{cases} \quad [30]$$

D. Large-*N* Steady-State Fitness Statistics of the Simple Star Graph. Here, we derive the steady-state statistics for the star graph (without self-loops, unweighted) for large, but finite, n $(=N-1)$ under temperature initialization. To do so, we work with the uniform mutational offspring fitness distribution. In that case, from Eq. **4**, we know that the steady-state fitness distribution of a graph depends only on the fixation probabilities. Therefore, to derive the steady-state distribution for the star graph in the limit of large n, we first approximate the temperature-initialized fixation probability, $\phi^{\mathcal{T}}_{G_{n+1}(\lambda=1,\delta=1)}(f',f)$. Unless specified, we use the shorthand G_{n+1} to denote a star graph (without self-loops, unweighted) with n leaves. To approximate the fixation probability, we first set $\lambda=1$ and $\delta=1$ and then perform a Taylor expansion of Eq. **28** around $1/n=0$, leading to

$$\phi^{\mathcal{T}}_{G_{n+1}}(f',f)=\begin{cases}\frac{\left(\frac{f'}{f}-1\right)\left(1+\frac{f'}{f}\right)^2}{n\left(\frac{f'}{f}\right)^2}+\mathcal{O}\left(\frac{1}{n^2}\right), & \text{if } f'>f,\\ \frac{\left(1-\frac{f'}{f}\right)\left(1+\frac{f'}{f}\right)^2}{n\left(\frac{f'}{f}\right)^2}\left(\frac{f'}{f}\frac{\left(n\frac{f'}{f}+1\right)}{\left(\frac{f'}{f}+n\right)}\right)^n+\mathcal{O}\left(\frac{1}{n^2}\right), & f'\leq f.\end{cases} \quad [31]$$

Thus, for large N, $\phi^{\mathcal{T}}_{G_{n+1}}(f',f)\sim 1/n$, which makes the star graph a suppressor of selection under temperature initialization for infinite n. This is in accordance with the infinite n limit of $\phi^{\mathcal{T}}_{G_{n+1}(\lambda=1,\delta=1)}(f',f)$ that we saw in the previous section.

To make use of the approximated fixation probability shown in Eq. **31**, we write the denominator appearing in the steady-state distribution (Eq. **4**) as

$$\int_{f_{\min}}^{f_{\max}}\mathrm{d}f'\,\frac{\phi^{\mathcal{T}}_{G_{n+1}}(f',f)}{\phi^{\mathcal{T}}_{G_{n+1}}(f,f')}=\int_{f_{\min}}^{f}\mathrm{d}f'\,\underbrace{\frac{\phi^{\mathcal{T}}_{G_{n+1}}(f',f)}{\phi^{\mathcal{T}}_{G_{n+1}}(f,f')}}_{\Gamma_3}+\int_{f}^{f_{\max}}\mathrm{d}f'\,\underbrace{\frac{\phi^{\mathcal{T}}_{G_{n+1}}(f',f)}{\phi^{\mathcal{T}}_{G_{n+1}}(f,f')}}_{\Gamma_4}. \quad [32]$$

Notice that the $1/n$ scaling of the fixation probabilities responsible for the suppression of selection for a large-sized star graph drops out in both the integrands. Putting it differently, the steady-state fitness decreasing contribution coming from the poor beneficial mutant fixation profile has been compensated by the deleterious mutant fixation profile. As a side remark, the steady-state statistics for a general graph G is invariant under the scaling of the fixation profile $\phi^{\mathcal{I}}_G$ by any n-dependent bounded function $g(n)$, i.e., $P^*_G[g\phi^{\mathcal{I}}_G]=P^*_G[\phi^{\mathcal{I}}_G]$.

Now, for the integrand Γ_3, $f'\leq f$, whereas for Γ_4, $f'>f$. The integrand Γ_3 can be simplified as,

$$\begin{aligned}\Gamma_3&=\frac{\frac{\left(1-\frac{f'}{f}\right)\left(1+\frac{f'}{f}\right)^2}{n\left(\frac{f'}{f}\right)^2}\left(\frac{f'}{f}\frac{\left(n\frac{f'}{f}+1\right)}{\left(\frac{f'}{f}+n\right)}\right)^n}{\frac{\left(1-\frac{f'}{f}\right)\left(1+\frac{f'}{f}\right)^2}{n\frac{f'}{f}}}\\&=\left(\frac{f'}{f}\right)^{n-1}\left(\frac{n\frac{f'}{f}+1}{\frac{f'}{f}+n}\right)^n\\&=\left(\frac{f'}{f}\right)^{2n-1}\left(\frac{1+\frac{f}{nf'}}{1+\frac{f'}{nf}}\right)^n\\&\approx\left(\frac{f'}{f}\right)^{2n-1}\exp\left(\frac{f}{f'}-\frac{f'}{f}\right),\end{aligned} \quad [33]$$

where in the last line, we have used the limit definition of the exponential function by assuming large n, $\exp(x)\approx(1+\frac{x}{n})^n$ for large n. Furthermore, if we assume $f,f'\ll n$, the dominant contribution to the integrand Γ_3 then comes from the n dependent term, and, thus, Γ_3 simplifies to

$$\Gamma_3\approx\left(\frac{f'}{f}\right)^{2n-1}. \quad [34]$$

Similarly, Γ_4 takes the form,

$$\Gamma_4\approx\left(\frac{f'}{f}\right)^{2n-1}. \quad [35]$$

Since the integrands Γ_3 and Γ_4 are identical, Eq. **32** reduces to

$$\begin{aligned}\int_{f_{\min}}^{f_{\max}}\mathrm{d}f'\,\frac{\phi^{\mathcal{T}}_{G_{n+1}}(f',f)}{\phi^{\mathcal{T}}_{G_{n+1}}(f,f')}&=\int_{f_{\min}}^{f_{\max}}\mathrm{d}f'\,\left(\frac{f'}{f}\right)^{2n-1}\\&=\frac{f_{\max}^{2n}-f_{\min}^{2n}}{2n}\frac{1}{f^{2n-1}}.\end{aligned} \quad [36]$$

This gives us the steady-state fitness distribution for the star graph in the large-n limit,

$$P^*_{G_{n+1}}(f) = \frac{2n}{f_{\max}^{2n} - f_{\min}^{2n}} f^{2n-1}. \quad [37]$$

With this, we can now compute the average steady-state fitness for the star graph in the large-n limit,

$$\begin{aligned} \langle f \rangle^*_{G_{n+1}} &= \int \mathrm{d}f \; f P^*_{G_{n+1}}(f) \\ &= \frac{2n}{f_{\max}^{2n} - f_{\min}^{2n}} \int_{f_{\min}}^{f_{\max}} \mathrm{d}f \; f \cdot f^{2n-1} \\ &= \frac{2n}{2n+1} \frac{f_{\max}^{2n+1} - f_{\min}^{2n+1}}{f_{\max}^{2n} - f_{\min}^{2n}} \\ &\approx f_{\max}, \end{aligned} \quad [38]$$

where in the last line, we have again made use of the large-n approximation. Therefore, the steady-state average fitness for the star graph asymptotes to $f_{\max}$ for large population size. In Fig. 3*C*, we have seen that for small n, the star graph attains higher steady-state average fitness in the mutation–selection balance than the complete graph. To see if this holds for large n as well, we study the quantity $\langle f \rangle^*_{G_{n+1}} - \langle f \rangle^*_C$.

$$\begin{aligned} \langle f \rangle^*_{G_{n+1}} - \langle f \rangle^*_C =& \frac{2n}{2n+1} \frac{f_{\max}^{2n+1} - f_{\min}^{2n+1}}{f_{\max}^{2n} - f_{\min}^{2n}} \\ &- \frac{n+1}{n+2} \frac{f_{\max}^{n+2} - f_{\min}^{n+2}}{f_{\max}^{n+1} - f_{\min}^{n+1}} \\ =& \frac{f_{\max}}{2n} + \mathcal{O}\left(\frac{1}{n^2}\right). \end{aligned} \quad [39]$$

Because $\frac{f_{\max}}{2n} > 0$, in the large-n limit, the star graph—a suppressor of fixation—attains higher steady-state average fitness in the mutation–selection balance than the complete graph.

E. Mixing Time for Single Rooted Graphs. For any one-rooted network with self-loops, we can use Eq. **2** to find an exact expression for the full temporal statistics, $P_G(f,t)$, when mutational fitness jump distribution is uniform. To do so, we first note that the fixation probabilities become independent of fitness values, $\phi^{\mathcal{T}}_G(f,f') = \phi^{\mathcal{T}}_G(f',f) = \frac{\mathcal{T}_r}{N}$, where $\mathcal{T}_r$ is the temperature of the root node. Substituting the fixation probabilities in Eq. **2**, and using the normalization condition for $P_G(f',t)$, we obtain a first-order ordinary differential equation for $P_G(f,t)$ in time,

$$\frac{\partial P_G(f,t)}{\partial t} = \frac{\mu \mathcal{T}_r}{N} \left(\frac{1}{f_{\max} - f_{\min}} - P_G(f,t) \right). \quad [40]$$

Solving this equation, we obtain

$$P_G(f,t) = \frac{1}{f_{\max} - f_{\min}} - \left(\frac{1}{f_{\max} - f_{\min}} - P_G(f,0) \right) e^{-\frac{\mu \mathcal{T}_r t}{N}}. \quad [41]$$

From this expression, we find that in the limit $t \to \infty$, the dynamics for a single rooted graph becomes completely random. That is, at long times, a population spends equal time in all the fitness states. On comparing with Eq. **7**, we find that the mixing time—i.e., the number of mutations required to reach the steady-state—for these graphs scales as $\frac{N}{\mathcal{T}_r \mu}$.

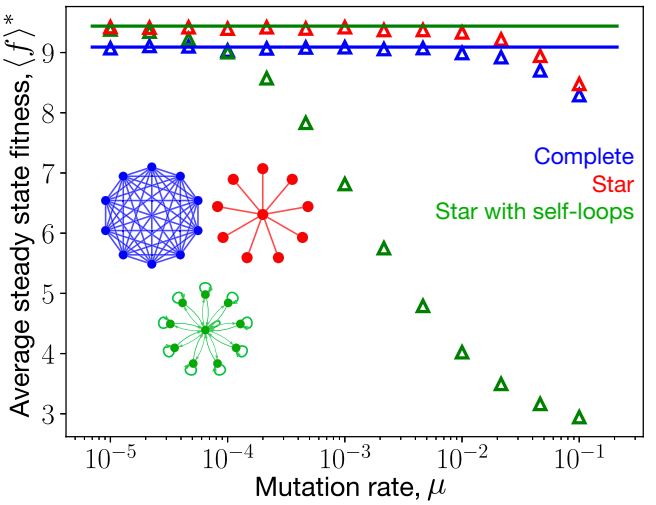

Fig. 7. Deviation from the low mutation rate approximation. Using the Moran Bd simulations, the average steady-state fitness attained in the mutation–selection balance is plotted as a function of mutation rate, which is identical to the mutation probability with a single Moran Bd update step as the unit of time. Parameters are the same as those of Fig. 3. We observe that the self-looped star is much more restrictive to low mutation approximation than the other two graphs. The reason for this is its much higher fixation time. On the other hand, for the star graph, the low mutation approximation is valid in a similar regime as for the complete graph. Again, this is due to its fixation time being the same order as the complete graph under temperature initialization. Outside the weak mutation regime, the star continues to maintain higher steady-state average fitness, while the steady-state fitness for the self-looped star graph, an amplifier of selection, falls rapidly.

As a result, the mixing time for a single rooted graph can be modulated by changing the temperature of the root node. Moreover, the average fitness for the case of a single-rooted graph (root with self-loops) with temperature $\mathcal{T}_r$ can be found using Eq. **41**,

$$\langle f(t) \rangle_G = \frac{f_{\max} + f_{\min}}{2} - \left(\frac{f_{\max} + f_{\min}}{2} - \langle f(0) \rangle_G \right) e^{-\frac{\mu \mathcal{T}_r t}{N}}. \quad [42]$$

In the limit $t \to \infty$, the average fitness converges to the average of the fitness domain. We also note that the steady state for single rooted graphs (with self-loops) is independent of the choice of phenotype-fitness map—simply because the fixation probability for these graphs does not depend on fitness.

F. Deviation from the Low Mutation Rate Approximation. The weak mutation approximation works well if the time between two successive mutation events is much longer than the average time it takes for the fixation or extinction of a mutant. Thus, there exists an upper bound for the mutation rate, above which the dynamics starts showing deviation from the weak mutation approximation. For the case of an evolutionary game in a well-mixed population, this upper bound for the mutation rate is derived in ref. 50. The validity of the low mutation rate approximation depends not only on the mutation rates, but also the fixation time. Previous studies have indicated that, compared to the complete graph, the graphs with higher fixation times call for lower mutation rates for this approximation to hold (25, 31, 33). Here, we verify these predictions. In Fig. 7, we find that, compared to the complete graph, the self-looped star graph is very restrictive to the low-mutation-rate approximation. On the other hand, in the star graph, a suppressor of fixation, the threshold mutation rate value for the deviation from the low mutation rate approximation is similar to the complete graph. This may be unexpected, as for uniform

initialization, the fixation time for the star graph is an order of magnitude higher than for the complete graph. However, here, we are dealing with temperature-initialized sequential dynamics, where the fixation time for the star graph becomes almost the same as that of the complete graph, at least for small population sizes, while the fixation times for self-looped star remains much higher. Also, the star not only attains a higher steady-state average fitness than the complete graph under the weak mutation approximation, but also outside the weak mutation regime. In contrast, the self-looped star graph, an amplifier of selection, performs poorly outside the weak mutation rate regime by attaining lower steady-state average fitness than the complete graph. Therefore, in general, an amplifier of selection does not maximize fitness.

Data, Materials, and Software Availability. Code to reproduce figures and underlying data (Mathematica files/Jupyter notebooks) has been deposited in GitLab (https://gitlab.gwdg.de/mpievolbio-scicomp/DynamicsOnGraphs_LowMutationRate.git) (51).

ACKNOWLEDGMENTS. We are grateful to the members of the Evolutionary Theory department and the Dynamics of Social Behavior group for continuous discussions. We thank Carsten Fortmann-Grote for assistance with computer cluster usage.

1. E. Lieberman, C. Hauert, M. A. Nowak, Evolutionary dynamics on graphs. *Nature* **433**, 312–316 (2005).
2. M. Broom, J. Rychtář, B. Stadler, Evolutionary dynamics on small-order graphs. *J. Interdiscip. Math.* **12**, 129–140 (2009).
3. T. Monk, P. M. P. Green, Martingales and fixation probabilities of evolutionary graphs. *Proc. R. Soc. A Math. Phys. Eng. Sci.* **470**, 20130730 (2014).
4. L. Hindersin, B. Wu, A. Traulsen, J. García, Computation and simulation of evolutionary game dynamics in finite populations. *Sci. Rep.* **9**, 6946 (2019).
5. Y. P. Kuo, C. Nombela-Arrieta, O. Carja, A theory of evolutionary dynamics on any complex spatial structure. bioRxiv [Preprint] (2021). https://www.biorxiv.org/content/10.1101/2021.02.07.430151v1. Accessed 10 July 2022.
6. J. Tkadlec, A. Pavlogiannis, K. Chatterjee, M. A. Nowak, Limits on amplifiers of natural selection under death-birth updating. *PLOS Comput. Biol.* **16**, e1007494 (2020).
7. M. Kimura, Evolutionary rate at the molecular level. *Nature* **217**, 624–626 (1968).
8. D. M. McCandlish, C. L. Epstein, J. B. Plotkin, Formal properties of the probability of fixation: Identities, inequalities and approximations. *Theor. Popul. Biol.* **99**, 98–113 (2015).
9. M. A. Nowak, *Evolutionary Dynamics: Exploring the Equations of Life* (Harvard University Press, Cambridge, MA, 2006).
10. S. Giaimo, J. Arranz, A. Traulsen, Invasion and effective size of graph-structured populations. *PLOS Comput. Biol.* **14**, e1006559 (2018).
11. L. Hindersin, A. Traulsen, Most undirected random graphs are amplifiers of selection for birth-death dynamics, but suppressors of selection for death-birth dynamics. *PLOS Comput. Biol.* **11**, e1004437 (2015).
12. D. L. Hartl, C. H. Taubes, Towards a theory of evolutionary adaptation. *Genetica* **102–103**, 525–533 (1998).
13. S. Yagoobi, H. Yousefi, K. A. Samani, Mutation-selection stationary distribution in structured populations. *Phys. Rev. E* **98**, 042301 (2018).
14. A. McAvoy, B. Adlam, B. Allen, M. A. Nowak, Stationary frequencies and mixing times for neutral drift processes with spatial structure. *Proc. R. Soc. A Math. Phys. Eng. Sci.* **474**, 20180238 (2018).
15. T. Antal, S. Redner, V. Sood, Evolutionary dynamics on degree-heterogeneous graphs. *Phys. Rev. Lett.* **96**, 188104 (2006).
16. M. Newman, *Networks* (Oxford University Press, Oxford, UK, 2018).
17. L. Hindersin, B. Werner, D. Dingli, A. Traulsen, Should tissue structure suppress or amplify selection to minimize cancer risk? *Biol. Direct* **11**, 41 (2016).
18. B. Allen *et al.*, Fixation probabilities in graph-structured populations under weak selection. *PLOS Comput. Biol.* **17**, e1008695 (2021).
19. K. Kaveh, N. L. Komarova, M. Kohandel, The duality of spatial death-birth and birth-death processes and limitations of the isothermal theorem. *R. Soc. Open Sci.* **2**, 140465 (2015).
20. B. Adlam, K. Chatterjee, M. A. Nowak, Amplifiers of selection. *Proc. R. Soc. A Math. Phys. Eng. Sci.* **471**, 20150114 (2015).
21. D. M. McCandlish, A. Stoltzfus, Modeling evolution using the probability of fixation: History and implications. *Q. Rev. Biol.* **89**, 225–252 (2014).
22. C. W. Gardiner, *Handbook of Stochastic Methods*, *Springer Series in Synergistics*, vol. 13 (Springer, Berlin, ed. 3, 2004).
23. N. van Kampen, *Stochastic Processes in Physics and Chemistry* (North Holland, Amsterdam, 2007).
24. G. Sella, A. E. Hirsh, The application of statistical physics to evolutionary biology. *Proc. Natl. Acad. Sci. U.S.A.* **102**, 9541–9546 (2005).
25. J. Tkadlec, A. Pavlogiannis, K. Chatterjee, M. A. Nowak, Fast and strong amplifiers of natural selection. *Nat. Commun.* **12**, 4009 (2021).
26. J. H. Gillespie, A simple stochastic gene substitution model. *Theor. Popul. Biol.* **23**, 202–215 (1983).
27. H. A. Orr, The genetic theory of adaptation: A brief history. *Nat. Rev. Genet.* **6**, 119–127 (2005).
28. A. Pavlogiannis, J. Tkadlec, K. Chatterjee, M. A. Nowak, Construction of arbitrarily strong amplifiers of natural selection using evolutionary graph theory. *Commun. Biol.* **1**, 71 (2018).
29. D. A. Levin, Y. L. Peres, E. Wilmer, *Markov Chains and Mixing Times* (American Mathematical Society, Providence, RI, 2009).
30. C. Hadjichrysanthou, M. Broom, J. Rychtář, Evolutionary games on star graphs under various updating rules. *Dyn. Games Appl.* **1**, 386–407 (2011).
31. M. Frean, P. B. Rainey, A. Traulsen, The effect of population structure on the rate of evolution. *Proc. Biol. Sci.* **280**, 20130211 (2013).
32. M. Möller, L. Hindersin, A. Traulsen, Exploring and mapping the universe of evolutionary graphs identifies structural properties affecting fixation probability and time. *Commun. Biol.* **2**, 137 (2019).
33. J. Tkadlec, A. Pavlogiannis, K. Chatterjee, M. A. Nowak, Population structure determines the tradeoff between fixation probability and fixation time. *Commun. Biol.* **2**, 138 (2019).
34. J. Cairns, Mutation selection and the natural history of cancer. *Nature* **255**, 197–200 (1975).
35. M. A. Nowak, F. Michor, Y. Iwasa, The linear process of somatic evolution. *Proc. Natl. Acad. Sci. U.S.A.* **100**, 14966–14969 (2003).
36. P. P. Chakraborty, L. R. Nemzer, R. Kassen, Experimental evidence that metapopulation structure can accelerate adaptive evolution. bioRxiv [Preprint] (2021). https://www.biorxiv.org/content/10.1101/2021.07.13.452242v1. Accessed 10 July 2022.
37. S. van Vliet, C. Hauert, K. Fridberg, M. Ackermann, A. Dal Co, Global dynamics of microbial communities emerge from local interaction rules. *PLOS Comput. Biol.* **18**, e1009877 (2022).
38. G. W. Constable, A. J. McKane, Population genetics on islands connected by an arbitrary network: An analytic approach. *J. Theor. Biol.* **358**, 149–165 (2014).
39. B. Allen *et al.*, Transient amplifiers of selection and reducers of fixation for death-birth updating on graphs. *PLOS Comput. Biol.* **16**, e1007529 (2020).
40. S. Yagoobi, A. Traulsen, Fixation probabilities in network structured meta-populations. *Sci. Rep.* **11**, 17979 (2021).
41. L. Marrec, I. Lamberti, A. F. Bitbol, Toward a universal model for spatially structured populations. *Phys. Rev. Lett.* **127**, 218102 (2021).
42. A. McAvoy, B. Allen, Fixation probabilities in evolutionary dynamics under weak selection. *J. Math. Biol.* **82**, 14 (2021).
43. T. Monk, Martingales and the fixation probability of high-dimensional evolutionary graphs. *J. Theor. Biol.* **451**, 10–18 (2018).
44. M. Askari, K. A. Samani, Analytical calculation of average fixation time in evolutionary graphs. *Phys. Rev. E Stat. Nonlin. Soft Matter Phys.* **92**, 042707 (2015).
45. B. Ottino-Löffler, J. G. Scott, S. H. Strogatz, Takeover times for a simple model of network infection. *Phys. Rev. E* **96**, 012313 (2017).
46. D. Hathcock, S. H. Strogatz, Fitness dependence of the fixation-time distribution for evolutionary dynamics on graphs. *Phys. Rev. E* **100**, 012408 (2019).
47. T. Monk, A. van Schaik, Wald's martingale and the conditional distributions of absorption time in the Moran process. *Proc. Math. Phys. Eng. Sci.* **476**, 20200135 (2020). Correction in: *Proc. Math. Phys. Eng. Sci.* **476**, 20200731 (2020).
48. Y. P. Kuo, O. Carja, Evolutionary graph theory beyond pairwise interactions: Higher-order network motifs shape times to fixation in structured populations. bioRxiv [Preprint] (2021). https://www.biorxiv.org/content/10.1101/2021.06.26.450017v1. Accessed 10 July 2022.
49. T. Monk, A. van Schaik, Martingales and the fixation time of evolutionary graphs with arbitrary dimensionality. *R. Soc. Open Sci.* **9**, 220011 (2022).
50. B. Wu, C. S. Gokhale, L. Wang, A. Traulsen, How small are small mutation rates? *J. Math. Biol.* **64**, 803–827 (2012).
51. N. Sharma, A. Traulsen, DynamicsOnGraphs_LowMutationRate. GitLab. https://gitlab.gwdg.de/mpievolbioscicomp/DynamicsOnGraphs_LowMutationRate.git. Deposited 9 July 2022.